

Computing the eigenstate localisation length from Localisation Landscape Theory

S.S. Shamailov^{1*}, D.J. Brown¹, T.A. Haase¹, M.D. Hoogerland¹

¹ Dodd-Walls Centre for Photonic and Quantum Technologies, Department of Physics,
University of Auckland, Private Bag 92019, Auckland 1142, New Zealand.

* sophie.s.s@hotmail.com

September 10, 2021

Abstract

While Anderson localisation is largely well-understood, its description has traditionally been rather cumbersome. A recently-developed theory – Localisation Landscape Theory (LLT) – has unparalleled strengths and advantages, both computational and conceptual, over alternative methods. To begin with, we demonstrate that the localisation length cannot be conveniently computed starting directly from the exact eigenstates, thus motivating the need for the LLT approach. Then, we reveal the physical significance of the effective potential of LLT, justifying the crucial role it plays in our new method. We proceed to use LLT to calculate the localisation length, as defined by the length-scale of exponential decay of the eigenstates, (manually) testing our findings against exact diagonalisation. We place our computational scheme in context by explaining the connection to the more general problem of multidimensional tunnelling and discussing the approximations involved. The conceptual approach behind our method is not restricted to a specific dimension or noise type and can be readily extended to other systems.

Contents

1	Introduction	2
2	System of interest	4
3	Exact diagonalisation	5
4	The effective potential	8
5	Eigenstate localisation length	11
5.1	Outline of the LLT method	14
5.2	Test of decay constants	17
5.3	Effect of parameters	17
6	Multidimensional tunnelling	21

7	Conclusions and future work	23
	References	24

1 Introduction

Anderson localisation [1] is a universal wave interference phenomenon, whereby transport (i.e. wave propagation) is suppressed in a disordered medium due to dephasing upon many scattering events from randomly-positioned obstacles. This can be understood from Feynman's interpretation of quantum mechanics, where one must sum over all possible paths from the initial to the final points of interest to obtain the total transmission probability. The random positions of the scatterers guarantee dephasing between the different paths, leading to an attenuation of the amplitude of the wavefunction. First discovered in the context of quantised electron conduction and spin diffusion [2], Anderson localisation of particles thus provides direct evidence for the quantum-mechanical nature of the universe at a small scale.

In particular, Anderson localisation is characterised by an exponential decay in the tails of the wavefunction with a length scale known as the localisation length [2]. The computation of this key variable is not straight-forward. For continuous systems, a rough estimate can be obtained by setting the renormalised diffusion coefficient, derived in the limit of weak scattering where it is only slightly reduced from its classical value, to zero [3, 4]. While the resulting analytical formula is not expected to be accurate, it is of course convenient, and is thus used by many researchers [5–8]. The diffusive picture is in general often employed to describe Anderson localisation, even though it is strictly inapplicable in this limit [6, 8]. A rigorous calculation can be performed using Green's functions [3, 4, 9], but it requires many assumptions regarding the nature of the disorder and is quite involved. On the other hand, Green's functions can be used to extend the classical diffusive picture into the weakly-localised regime by computing the correction to the diffusion coefficient [3, 4, 6], and even push this picture into the strongly localised limit by making the renormalised diffusion integral equation self-consistent [3, 4, 6, 10].

Another approach to obtain the localisation length is the Born approximation, commonly utilised for weak scattering [5, 7, 11]: here, one takes the total wave in the extended scattering body as the incident wave only, assuming that the scattered wave is negligibly small in comparison. Understandably, this method is inaccurate for strong disorder. Exact time-dependent simulations with the Schrödinger [5, 7, 12, 13] or Gross-Pitaevskii [14, 15] equations can be used instead, but this approach is very time-consuming and yields little insight into the physics. Finally, access to the localisation length directly through the eigenstates of the Hamiltonian is hampered by practical considerations (as we shall show below).

Other, more model-specific methods have also been employed in the literature: [16] solved the Schrödinger equation via a random walk on a hyperboloid, [17] derived a non-linear wave equation to extract the Lyapunov exponents corresponding to the linear problem of interest, [18] solved the kicked-rotor model analytically, and [19] derived analytical expressions relevant for the weak disorder limit.

For discrete models, a plethora of methods to calculate the localisation length likewise ex-

ists. The most renowned is of course the transfer matrix method, allowing for the calculation of Lyapunov exponents and thus the localisation length [20–28]. Such calculations have commonly been used to confirm the predictions of finite scaling theory [23, 26]. While often used together, transfer matrices and Lyapunov exponents have been combined with other elements to obtain the localisation length: the former with analytical continuation [29] to compute moments of resistance and the density of states, and the latter in a perturbative expansion, with numerical simulations of a quantum walker [30]. The Kubo-Greenwood formalism has also proved highly successful [23, 31, 32].

Green’s functions have been as invaluable for discrete systems as for continuous [9, 11, 12, 23, 33, 34], allowing for renormalisation techniques to be applied [34, 35], or alternatively scattering matrices, treated with the Dyson equation [9]. Out of these references, [33] examined the off-diagonal elements of the Green’s matrix as a localisation order parameter, [12] the distribution of eigenstates which was related to the spatial extent of the eigenstates, [9] the characteristic determinant related to the poles of the Green’s function, and Ref. [34] developed a renormalised perturbation expansion for the self energy. Recursion formulae encoding the exact solution [36, 37] can also sometimes allow one to calculate the localisation length (and the density of states [37]).

Out of the studies above, one-dimensional (1D) [5, 12, 16–18, 20–22, 29, 30, 33, 34, 36, 37] and two-dimensional (2D) [5–7, 9, 11, 13, 19–27, 35] models have been numerically explored far more thoroughly than three-dimensional (3D) [5, 26, 33], simply because of the increased computational requirements of higher-dimensional spaces. Possibly the most heavily studied model of localisation is the Anderson model, also known as the tight-binding Hamiltonian [3, 9, 11, 12, 21–26, 28, 29, 31, 33–36, 38–43], but other examples include the kicked rotor [18] (formally equivalent to the Anderson model), the Lloyd model [12, 20], the Peierls chain [37], a quantum walker [30], and the continuous Schrödinger equation [12, 13, 16], with either a speckle potential [6, 15], delta-function point scatterers [5, 9], or more realistic Gaussian scatterers [7].

Meantime, a break-through new theory – coined Localisation Landscape Theory (LLT) [44–50] – was developed recently, completely revolutionising the field. It allows for intuitive and transparent new insights into the physics, as well as a practical, efficient way of performing calculations. To give a brief overview, this theory relies on the construction of a function, the localisation landscape, which governs all the low-energy, localised physics. One can treat finite problems so that boundary effects are accounted for, and yet push the algorithms to very large system sizes, where alternative methods are completely impractical. The validity of this theory is not restricted to a specific noise type, making it widely applicable to a range of problems. An effective potential can be constructed, such that quantum interference effects can be captured instead by quantum tunnelling through this effective potential. One can predict the main regions of existence (referred to as “domains”) of the low-energy localised eigenstates, reconstruct the eigenstates on these domains, as well as compute the associated energy eigenvalues. Thus, Anderson localisation can be fully reinterpreted in this picture, including the energy dependence of the localisation length. Very recently, LLT has been used to support an experimental study of Anderson localisation [51].

In this paper, we search for a way to calculate the localisation length for an arbitrary disordered, continuous potential. We begin by showing that the localisation length cannot be efficiently extracted from the eigenstates of the Hamiltonian. From there, we turn to LLT, and directly reveal the physical significance of the effective potential, which justifies its use in the work that follows. Indeed, we demonstrate how the localisation length can be obtained from LLT, a method that can be applied to continuous systems with any potential (as long

as it satisfies the basic applicability requirements of LLT), for any strength of the disorder, and which will provide accurate results for a range of (reasonably low-lying) energies. Our description is in 2D, a 1D version is much simpler and can be implemented with no additional effort, while a 3D version can be eventually developed by a direct analogy.

Thus, we extend LLT by developing a method for the computation of the localisation length in 2D systems. The main achievement lies in finding an efficient way of evaluating the so-called “Agmon distance”, an exponential decay cost for crossing domain walls – barriers in the effective potential of LLT separating neighbouring domains. We discuss how our method fits in to the extensive literature on multidimensional tunnelling, and then test it against the results of exact diagonalisation.

For the rest of the article, familiarity with LLT is certainly helpful. This background knowledge can be obtained by reading the original papers [44–50], or a succinct review of the key facts found in [52] (we use the same notation here as in [52]). Note that the present article is one out of five related publications, available as a single, coherent report [52].

The paper is structured as follows. We begin by introducing the system of interest in section 2, and proceed to demonstrate what can and cannot be learned from an exact diagonalisation of the Hamiltonian in section 3. In section 4, we expose new aspects of the physical significance of the effective potential of LLT. Then, in section 5, we extend known LLT to calculate the localisation length, as defined by the length scale of exponential decay in the tails of the eigenstates of the Hamiltonian, and directly test the method by comparison to exact eigenstates. In the process, we develop a simple and practical approximation to multidimensional tunnelling, discussed in section 6, which has many potential applications in other contexts.

Conclusions are presented in section 7 and several ideas are discussed as directions for a possible forthcoming investigation. Details about our computational techniques and the numerical methods employed can be found in the appendices of [52].

2 System of interest

We consider a (non-interacting) particle of mass m confined to a 2D plane, whose motion is restricted to a rectangular region defined by $x \in [0, L]$ and $y \in [0, W]$ with Dirichlet boundary conditions. The particle moves in an external potential $V(x, y)$, taken as a sum of N_s randomly-placed Gaussian peaks of amplitude V_0 and standard deviation σ , as suggested in [7]. This system could be experimentally realised with cold atoms as in [14]. A more detailed description of the system can be found in [52].

Next, we must introduce a set of dimensionless units, to be used throughout the paper. Let ℓ be a typical physical length scale relevant for the problem (for example, $\ell \sim \sigma$). Lengths will be measured in units of ℓ , energy is units of $E_0 = \hbar^2/(2m\ell^2)$, and time in $t_0 = \hbar/E_0$. Typically, for a cold-atom experiment such as [14], $\ell \sim 1 \mu\text{m}$, $E_0 \sim 1 \text{ nK} \times k_B$, and $t_0 \sim 5 \text{ ms}$.

A key parameter characterising the disorder is the dimensionless density of the scatterers, referred to as the fill factor, f :

$$f = \frac{N_s \ell^2}{LW}. \quad (1)$$

3 Exact diagonalisation

Our overall aim is to predict the localisation length for the system in section 2. Since the system size is finite, the potential is continuous, and does not have the required statistics for the Green’s functions method to be helpful, we must search for an alternative approach. Now, the problem of interest is linear, so all the information is contained in the Hamiltonian and its spectrum. We therefore begin our investigation by directly diagonalising the Hamiltonian and inspecting the eigenstates and energies, with the goals of (a) gaining intuition for our system and (b) checking whether useful quantitative predictions may be readily obtained in this framework. Details on the numerical implementation are given in appendix A of [52].

In general, our results support the well-known fact that the localisation length increases with energy. We find that the localised eigenstates lie at low energies, and the degree of localisation decreases as the energy increases. This can be easily seen by eye when inspecting the eigenstates, plotting $|\psi|$. An example is shown in Fig. 1, depicting nine low-energy eigenstates for a particular noise realisation. Overall, as energy increases, the weight of the eigenstates spreads out over a larger area (see Fig. 3 of [44] for another example). This process, however, is not monotonic: occasionally we encounter very localised states with a fairly high energy, where most of the energy comes from the rapidly changing wavefunction rather than the spatial extent and the associated potential energy. Also quite intuitively, if f or V_0 are increased, the strength of localisation increases and the area within which the weight of the eigenstates is contained shrinks. Figure 2 demonstrates this by visually comparing the lowest energy eigenvector for different combinations of f and V_0 . We see that both the fill factor and the scatterer height are equally important parameters, influencing localisation properties just as strongly.

Increasing the width of the scatterers σ also leads to stronger localisation (not illustrated), because the area occupied by the Gaussian peaks increases, but the dependence on the scatterer width is not explored here. The shape of the scatterers also plays a role, of course, but as long as the (“volume”) integral over a single scatterer is kept constant, the specific functional form is expected to have a much weaker effect on the physics than f and V_0 . The shape of the scatterers influences the spectral properties of the disordered potential, the relation of which to a (possible) mobility edge could be investigated in the future.

Note that one may wonder whether the low-energy, localised states seen in Figs. 1 and 2 are simply trapped in local minima of the potential V , formed by surrounding Gaussian scatterers. This can be easily ruled out by visual inspection of the potential, as was in fact done in [44], confirming that the localised nature of these states arises from quantum interference and not classical trapping.

Next, let us consider how the localisation length may be extracted from the exact eigenstates of the Hamiltonian. By definition, the localisation length is the length scale on which the localised states decay exponentially, far away from the region where their main weight is concentrated. This decay can be seen in Fig. 2 as a change of colour from dark red to red to orange to yellow to green to blue, as the wavefunction gradually drops by orders of magnitude. The localisation length increases with energy, depends on the strength of the disorder, and should only be discussed in a configuration-averaged context.

If we inspect any one given eigenstate, assuming the energy is sufficiently low or localisation is strong enough, there is usually only one peak – one local maximum – in $|\psi|$. If we temporarily place our origin there and vary the azimuthal angle θ , then the curve $|\psi(r)|$ along

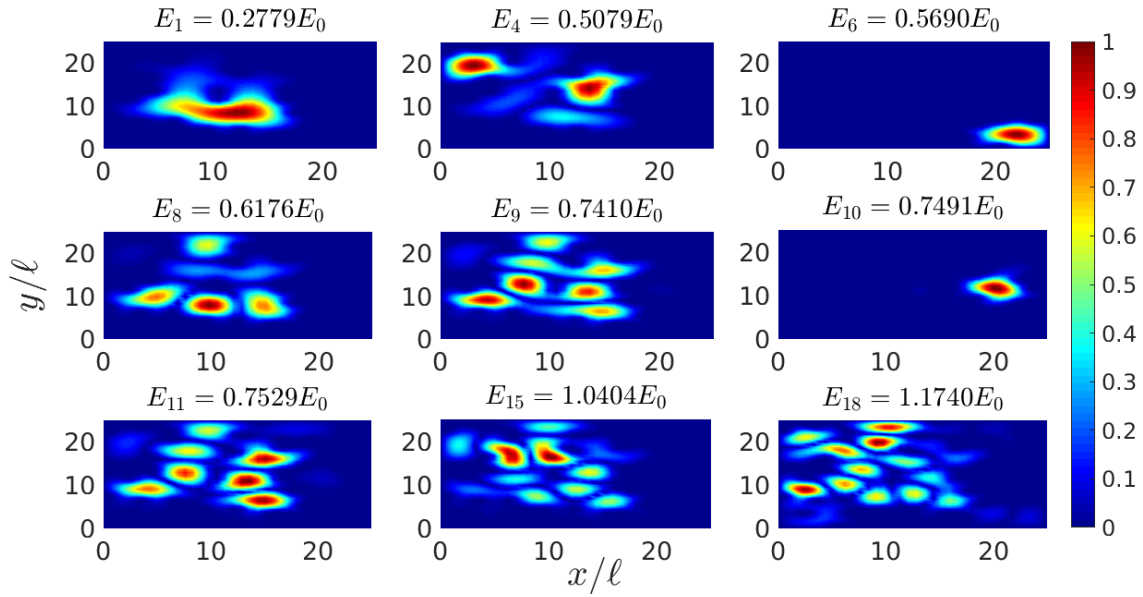


Figure 1: Nine low-energy eigenstates of the Hamiltonian for a given noise realisation with $L = W = 25\ell$, $f = 0.1$, $V_0 = 20E_0$, $\sigma = \ell/2$, showing the absolute value of the eigenstates as a colour-map. Note that all eigenstates are normalised such that the maximum is one so that the values can be read on the same colour bar. We see that overall, the spatial extent of the eigenstates increases with energy, quoted above each panel. However, occasionally, very localised states are encountered at higher energies, on account of the considerable kinetic energy such eigenstates carry.

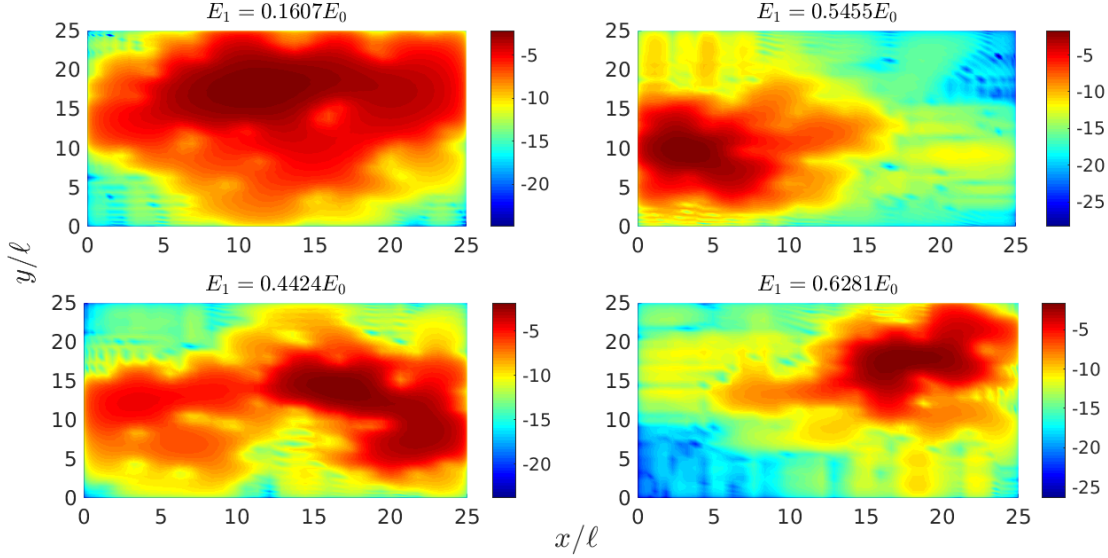


Figure 2: The lowest eigenstate of the Hamiltonian for some noise realisations with $L = W = 25\ell$ and $\sigma = \ell/2$, showing the logarithm of the absolute value of the eigenstates as a colour-map. Top left: $f = 0.1$, $V_0 = 10E_0$, top right: $f = 0.2$, $V_0 = 10E_0$, bottom left: $f = 0.1$, $V_0 = 20E_0$, bottom right: $f = 0.2$, $V_0 = 20E_0$. We observe that the degree of localisation is controlled both by the density of the scatterers and their height. The energy eigenvalue is quoted above each panel: it increases as the area of the (node-free) localised mode decreases.

different directions will certainly be different depending on θ . Still, we could average these curves over θ , and attempt fitting an exponential function to the tail of the resultant. If the peak is located in a corner of our rectangular system, for example, the average should only be taken over those angles along which one has reasonable extent along r .

However, as energy increases (or localisation decreases due to changes in parameters), the eigenstates develop a multi-peak structure: there are several “bumps” (see Fig. 1), and it is not clear where to place our origin. Furthermore, the energy eigenvalues are of course quantised, so any extracted localisation lengths from single-peak eigenstates need to be averaged over noise realisations, only using eigenstates of roughly the same energy (binning within a reasonable range). This makes such an approach very limited.

Now, a very common solution to this problem – heavily used in the literature (e.g. [13, 15, 53–57]) – is to compute the spatial variance of the localised states instead. Since we are working in 2D, we could tentatively examine the quantity

$$[\Delta x^2 \Delta y^2]^{1/4}, \quad (2)$$

where the variance along x is

$$\Delta x^2 = \langle x^2 \rangle - \langle x \rangle^2 = \int_0^L dx \int_0^W dy x^2 |\psi|^2 - \left[\int_0^L dx \int_0^W dy x |\psi|^2 \right]^2, \quad (3)$$

assuming the wavefunction is normalised to one, and Δy^2 is defined similarly.

Figure 3 shows a typical low energy eigenstate, plotting $|\psi|$ on a linear scale. The small-amplitude yet large-scale structure seen on the logarithmic plots of Fig. 2, capturing the exponential decay of the eigenstates away from their main region of existence, is completely invisible on such a plot. The variance-based length scale of (3) reports only on the width of the main peak seen in Fig. 3 – analogous to the full-width-at-half-maximum or the standard deviation of a Gaussian peak. It measures the size of the main bump, but carries no information on the exponential decay in the tails, and thus does not report on the localisation length, as such. We therefore advise caution when using the variance to quantify localisation properties, a common practice in the literature.

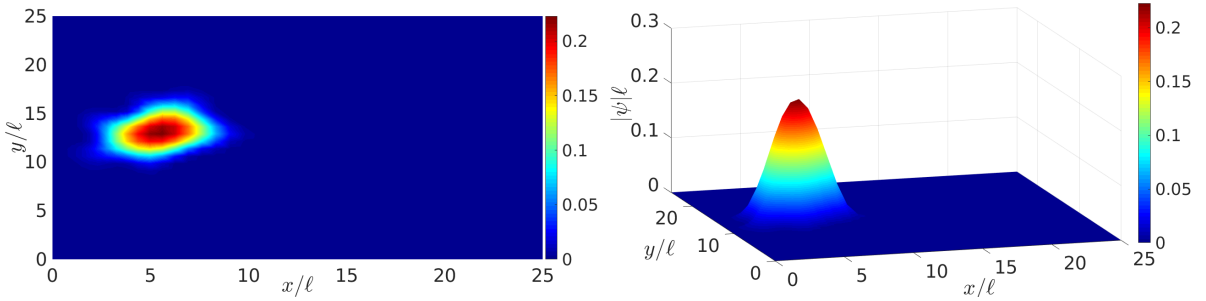


Figure 3: The lowest eigenstate of the Hamiltonian for a given noise realisation with $L = W = 25\ell$, $f = 0.2$, $V_0 = 20E_0$, $\sigma = \ell/2$, plotting $\ell|\psi|$ as a colour-map. The exponential decay away from the main region of existence of the eigenstate is unresolvable on a linear scale.

4 The effective potential

Since exact diagonalisation cannot help us to efficiently extract the localisation length, we turn to LLT for a solution. The method we develop heavily relies on the effective potential introduced in this theory, so before describing our approach, we explicitly validate the use of the effective potential in place of the real one in quantum-mechanical calculations. This is done in the present section.

The key object of LLT is the localisation landscape u , defined by the partial differential equation $Hu = 1$, where H is the Hamiltonian [44]. The associated effective potential W_E is simply given by $W_E = 1/u$. So far, LLT has produced several extremely useful results involving W_E which allow to make physical predictions for a system with real potential V – in our case, a disordered one. In particular, W_E controls the regions of localisation of the eigenstates at different energies, the density of states according to Weyl’s law, and the decay of the eigenstates through the valley lines of u according to the Agmon distance [47]. While the authors of [47, 48] motivate this remarkable success of the effective potential by an auxiliary wave equation, it appears that W_E may, to a good approximation, be able to replace V in the real Schrödinger equation, directly in the Hamiltonian. In this section we test to what degree this statement is valid.

First, we check whether the eigen-states and -energies of H with W_E are similar to those of H with V . To some extent, this is indeed the case, as demonstrated in Fig. 4. The energy spectrum seems very similar up to a global energy shift, while the eigenstates themselves are closely correlated for sufficiently low energies. Now, according to LLT, the valley lines of u –

collectively referred to as the “valley network” – divide the system into “domains” [44] (see the top panel of Fig. 7 for an illustrative example). The valley lines of u are of course the peak ranges of the effective potential, simply due to the inverse relationship between u and W_E . Therefore, the domains are surrounded by potential barriers and constitute the regions of localisation of low-energy eigenstates. Increasing the energy of the eigenstates enables the wavefunction to cross some of the potential barriers separating the domains and spread out further [47]. We find that for eigenstates that are localised to a handful of domains, involving fundamental local modes (i.e. there is only one density peak per domain), the similarity between eigenstates obtained using V and W_E is immediately obvious. Once localisation is weakened (e.g. by increasing the energy) to allow the occupation of many domains (possibly in excited local states), the correlation is lost. If Anderson localisation is strengthened (by increasing either or all of V_0 , f , σ), more low-energy eigenstates match between the spectra of H with V and H with W_E , and the agreement between the eigenstates is improved.

Returning to the energy shift between the eigenvalues in Fig. 4, the energies arising from diagonalising H with W_E always lie higher than their counterparts using H with V . Precisely the same trend is seen in Fig. 8 of [52], where the approximate eigenstates and eigenvalues are reconstructed from the localisation landscape u , avoiding numerical diagonalisation. This is very likely linked to the fact that in both cases, the approximate LLT eigenstates are a little more spread out than the exact. Since both V and W_E are positive functions, if an eigenstate has additional non-zero weight in some region of the system, its contribution would be to increase the potential energy. On the other hand, the more tightly-localised exact eigenstates would have more rapidly changing wavefunctions (as they decay to zero within a smaller area), and consequently, higher kinetic energy. It would thus appear that the difference in potential energy between exact and approximate eigenstates is larger than in the kinetic energy. Curiously, we observe that the energy shift seen in the top panel of Fig. 4 seems roughly equal to the value of W_E in its local basins, which was tested for many sets of parameters and several noise realisations. As a final note, we will see shortly that transmission in the effective potential always happens more readily than in the real. This may be explained by the observation that the eigenstates of H with W_E are somewhat more extended than the exact and have higher overlaps.

Next, let us consider time evolution (see appendix C of [52] for details on implementation). In light of the apparent physical significance of W_E , one would hope that a low energy wavefunction would evolve similarly in W_E and in V . We begin by placing a 2D Gaussian wavepacket¹ at the centre of the system. The initial condition (up to normalisation) reads

$$\psi = \exp\left(-\frac{r^2}{4\bar{\sigma}^2}\right), \quad (4)$$

where r is the radial coordinate centred on $(L/2, W/2)$, $\bar{\sigma} = \ell$ (for this example), and the state has energy $E \approx 0.5E_0$. Snap shots of the density are shown in Fig. 5 and reveal that indeed there is a visible similarity between the expansion of the wavefunction in the two potentials, although the state overlap drops quite rapidly. The effective potential generally allows for a better transmission than the real one, but a strong correlation is undeniable. Of course, as time goes on, the two evolving states become less similar. More faithful agreement can be obtained if localisation is strengthened by changing parameters, or if a lower energy wavefunction is used. An important aspect is the energy *distribution* of the wavefunction: in

¹The use of similar probing waves was independently suggested by [5] and used in the experiment [58].

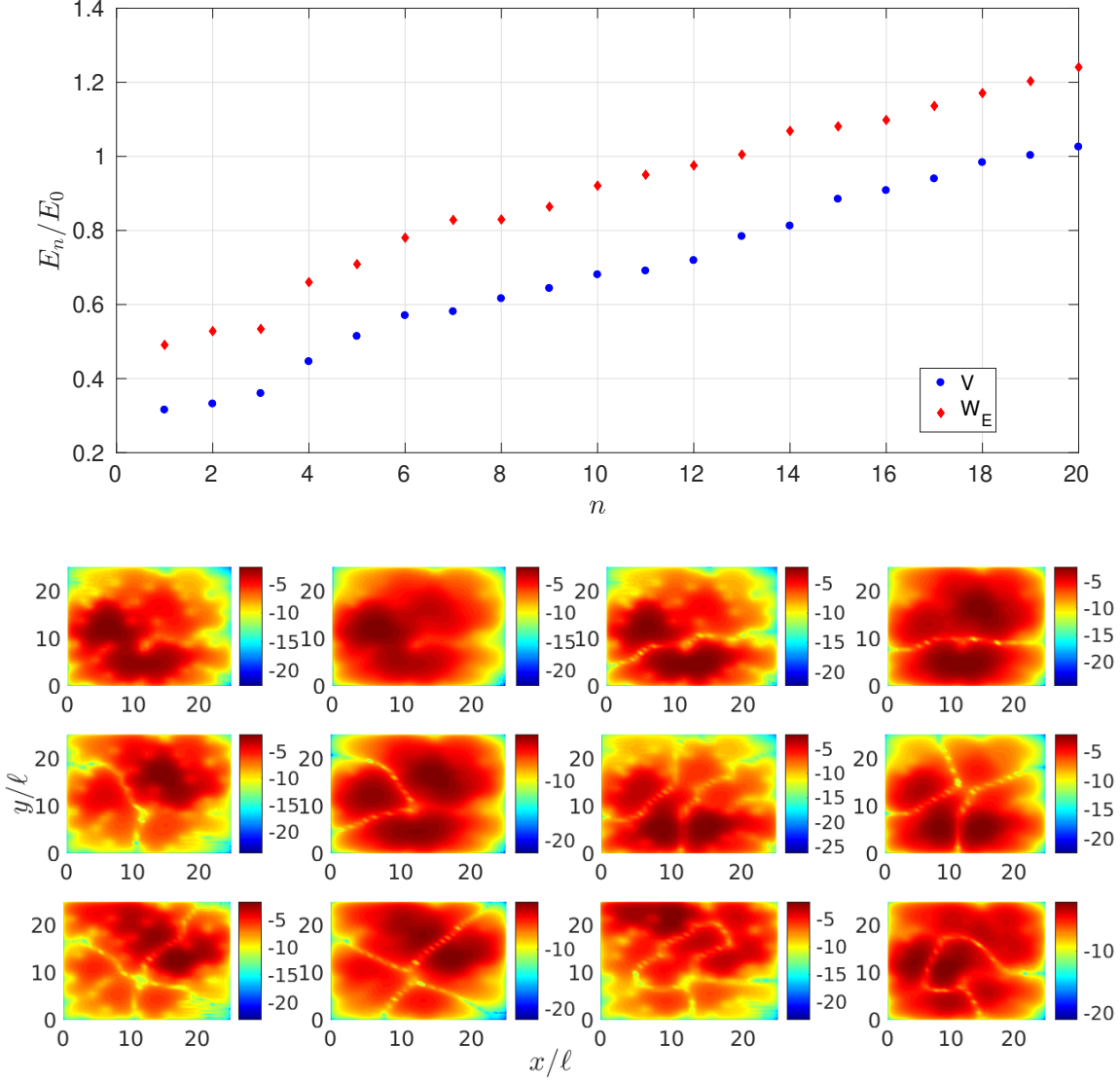


Figure 4: Low-energy eigenspectrum (top) and six of the lowest eigenstates with $L = W = 25\ell$, $f = 0.1$, $V_0 = 10E_0$, $\sigma = \ell/2$, showing the logarithm of the absolute value of the eigenstates as a colour-map (bottom). A direct comparison is drawn between the spectrum of the Hamiltonian with potential V and with W_E for the same noise realisation. The eigenvalues seem very similar, up to a global energy shift. In the bottom panel, going across the rows, we plot consecutively the n^{th} eigenstate using V and the n^{th} eigenstate using W_E , alternating between the potentials before increasing n . Thus the first and second panels can be directly compared, the third and fourth, etc. Up to the fifth eigenstate, the correlation between the mode shapes is clear. From the sixth eigenstate onward, there is no visible relation between the eigenmodes of the Hamiltonian with the two potentials.

our case here, the Gaussian is well-localised in position space, and therefore covers quite a broad momentum range. The behaviour of the high energy components will not be captured well by evolution in the effective potential, as we will see shortly.

In the case just considered, a wavefunction with stationary centre of mass (CoM) dynamics was initiated inside the disordered potential and allowed to expand into it. Now we introduce a transmissive scenario, studied in more detail in [52, 59]. First we have to slightly modify the geometry of the system we are examining. The region occupied by the potential scatterers remains precisely the same, $x \in [0, L]$, $y \in [0, W]$, but we add empty “reservoirs” on either side of the disorder where the potential is zero. These occupy $x \in [-R, 0]$, $y \in [0, W]$ (first reservoir, R_1) and $x \in [L, L + R]$, $y \in [0, W]$ (second reservoir, R_2). Usually, we choose $R = 30\ell$, just large enough to contain the initial condition that will be used. In the transmissive scenario, a wavefunction with CoM translation starts out in R_1 and goes through the disorder, finally arriving in R_2 .

The initial condition we will use in this set up is a 1D Gaussian wavepacket (Gaussian along x and uniform along y), which is fairly wide in position space and therefore has a rather localised energy distribution. The functional form is simply

$$\psi = \exp(-ik_0x) \exp\left[-\frac{(x + R/2)^2}{4\bar{\sigma}^2}\right], \quad (5)$$

where we leave out the normalisation constant. Figure 6 demonstrates the transmission of such a wavepacket with $\bar{\sigma} = 5\ell$, $k_0 = 1/\ell$, so that the momentum distribution is quite localised and the mean energy is $E \approx 1.17E_0$. Only at fairly late times significant differences arise between simulations using V and W_E for the potential, but the state overlap of the two wavefunctions decreases rather quickly. Whenever there is a strong difference between the two potentials, W_E always allows the wavefunction to spread / transmit farther and more freely. By varying k_0 we can easily change the energy of the probing wavepacket to address the question *under what conditions* can W_E approximate V well? The most accurate, although perhaps not so useful, answer we have been able to find is that this substitution works well as long as the dynamics are fairly localised. In other words, as energy increases, the validity of replacing V by W_E becomes questionable. Of course for weaker or sparser disorder, the range of energies where the replacement works well is much smaller.

To conclude, we have shown that W_E can to some degree replace V directly in the Schrödinger equation, both in terms of the eigen-values and -vectors, and in terms of time evolution in expansion and transmission. This understanding explains why general quantum-mechanical results based on the external potential serve to give useful physical predictions for a particle moving in V if W_E is used in these formulae instead of V .

5 Eigenstate localisation length

In this section we extend LLT to compute the localisation length, defined as the length scale of exponential decay in the tails of the eigenstates of the Hamiltonian. A combination of several LLT concepts allows for the development of a general methodology that can be applied to other systems, with other kinds of disorder, or in other dimensions. Technical details regarding the implementation can be found in appendix D of [52]. We explicitly test our ideas by direct comparison to exact eigenstates.

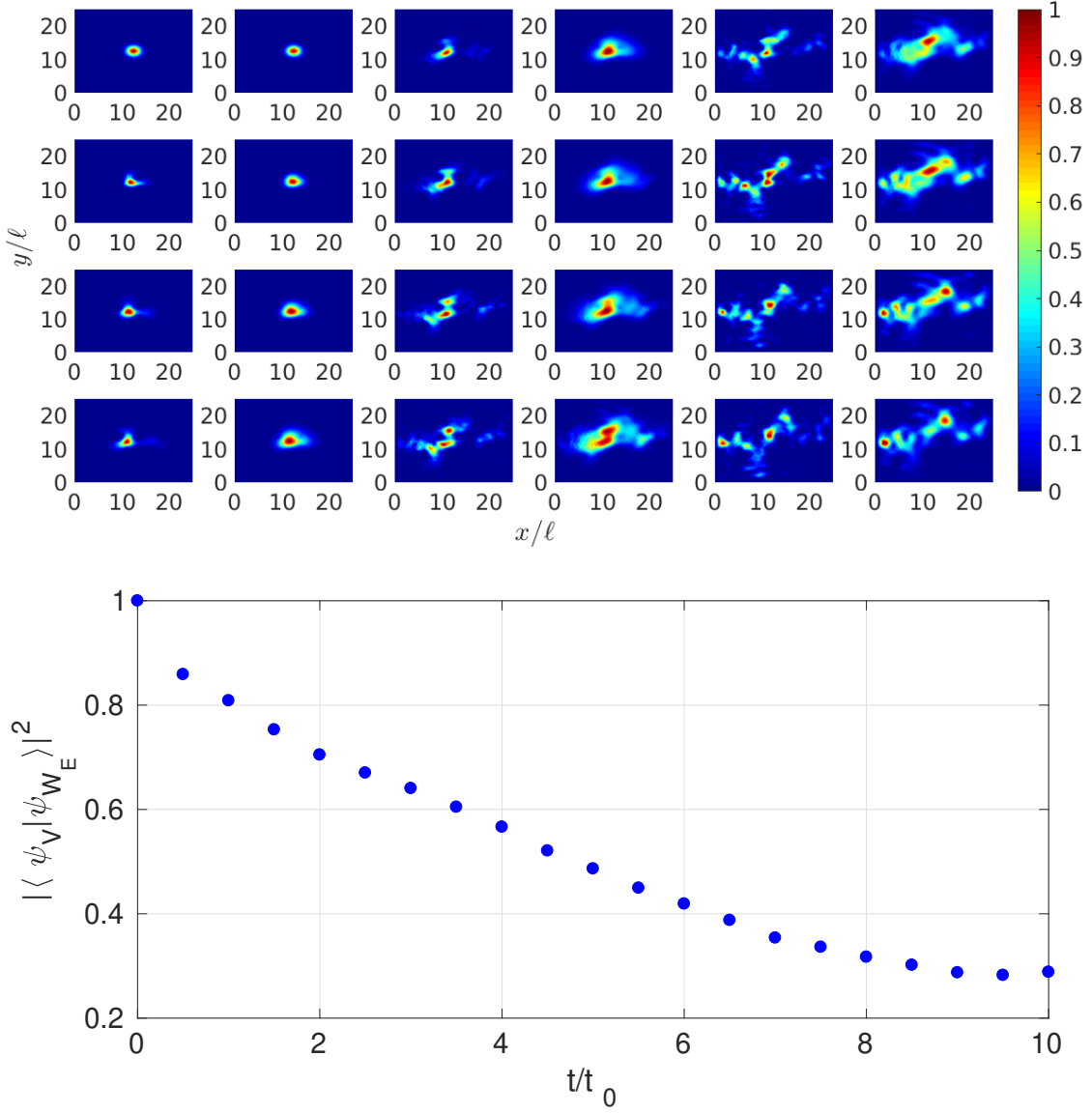


Figure 5: Top panel: Density profiles (all normalised such that the maximum is one so that the values can be read on the same colour bar) during time evolution of the initial condition (4) centred on $(L/2, W/2)$ with $\bar{\sigma} = \ell$, for the same parameters and noise realisation as used for Fig. 4. Columns 1,3,5 show evolution in V and 2,4,6 in W_E . Time starts at $t = 0$ and advances by $t_0/2$ in each snap shot, going down columns, then moving on to the next pair of columns. Indeed there is a visible similarity between the expansion of the wavefunction in the two potentials. Bottom panel: state overlap between the wavefunctions evolving in V and W_E as a function of time for the simulation in the top panel.

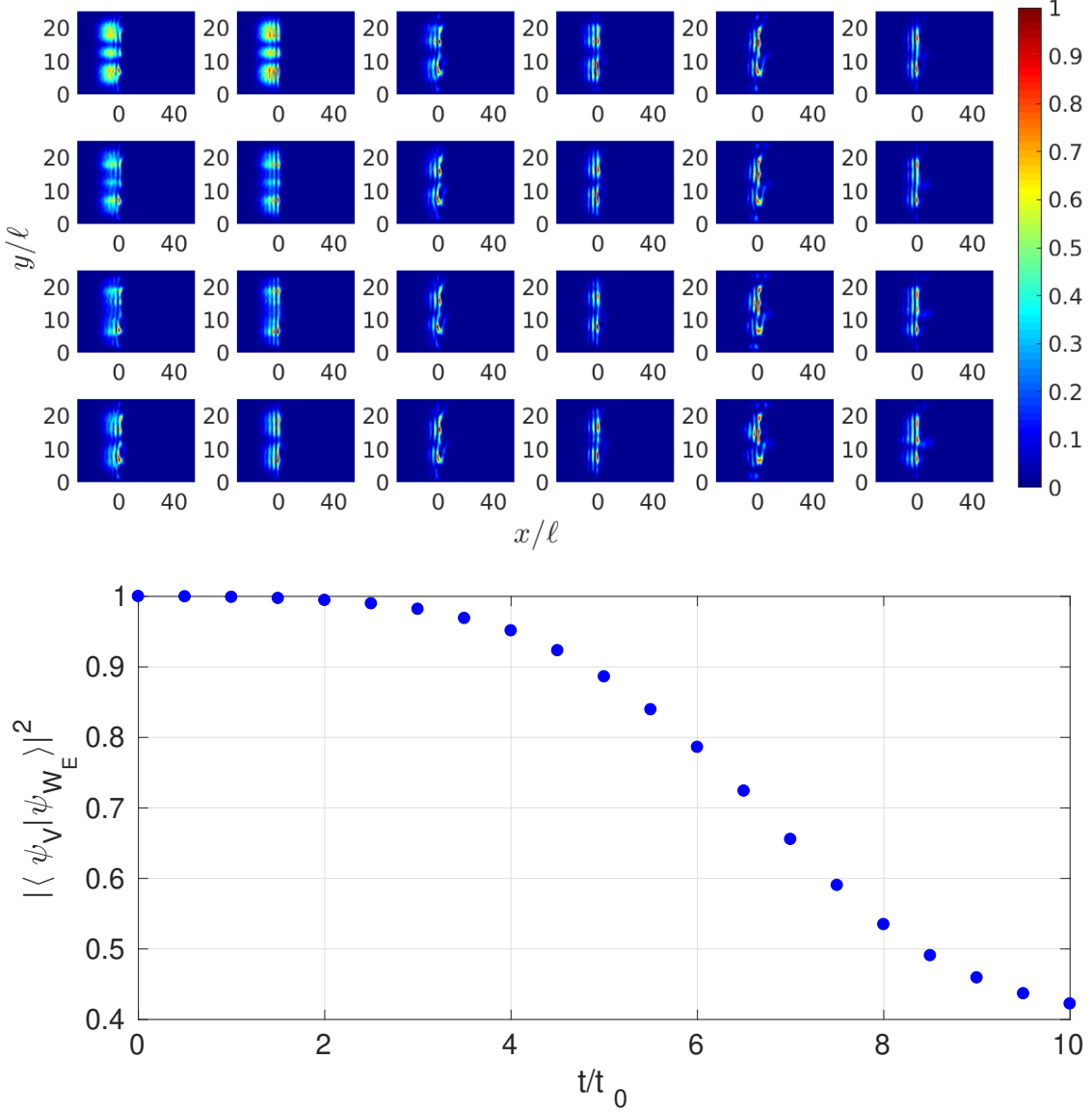


Figure 6: Top panel: Density profiles (all normalised such that the maximum is one so that the values can be read on the same colour bar) during time evolution of the initial condition (5) with $\bar{\sigma} = 5\ell$, $k_0 = 1/\ell$, $R = 30\ell$ for the same noise realisation and parameters as in Fig. 4. Columns 1,3,5 show evolution in V and 2,4,6 in W_E . Time starts at $t = 4$ (after the atoms enter the region with the scatterers) and advances by $t_0/2$ in each snap shot, going down columns, then moving on to the next pair of columns. Significant differences between evolution in the two potentials only become evident in the last four snap shots shown. Bottom panel: state overlap between the wavefunctions evolving in V and W_E as a function of time for the simulation in the top panel.

5.1 Outline of the LLT method

Recall that LLT has taught us that the low-energy eigenstates are localised inside domains of the valley network [44], and must tunnel through the peaks of the effective potential in order to spread to neighbouring domains. Within any given domain, there is nothing to induce exponential decay – the decay does not happen continuously (as commonly believed), but in discrete steps, every time the wavefunction crosses a valley line [47]. Furthermore, valley lines which are not part of a closed domain (referred to as “open” valley lines below) are irrelevant, as the wavefunction simply goes around them without losing amplitude.

Because of its prime importance to this section, we repeat here the definition of the energy-dependent quantity known as the Agmon distance [47, 48], which controls the decay of the eigenstates outside of their main domain of existence:

$$\rho_E(\mathbf{x}_0, \mathbf{x}) = \min_{\gamma} \left(\int_{\gamma} \Re \sqrt{2m[W_E(\mathbf{x}) - E]}/\hbar \, ds \right). \quad (6)$$

Because only the real part of the square root is used, the integrand is zero if E exceeds W_E at position \mathbf{x} . The integral should be minimised over all possible paths γ going from \mathbf{x}_0 to \mathbf{x} , and ds is the arc length. If we have an eigenstate peaked at position \mathbf{x}_0 inside some given domain, then it will have amplitude at position \mathbf{x} outside of this main domain bounded by

$$|\psi(\mathbf{x})| \lesssim |\psi(\mathbf{x}_0)| \exp[-\rho_E(\mathbf{x}_0, \mathbf{x})]. \quad (7)$$

As the authors of [47] point out, the formula (6) is commonly encountered in the context of the Wentzel–Kramers–Brillouin (WKB) approximation in 1D (and higher dimensions).

If we approximate the domains on average as circular in shape and denote the diameter D , then every distance D , the wavefunction undergoes a decay. The cost of crossing a valley line will be determined by the Agmon distance ρ_E , such that the amplitude of the wavefunction drops by a factor of $\exp(-\rho_E)$ on average every time. Combining these two quantities, we see that the localisation length is simply given by

$$\xi_E = D/\rho_E, \quad (8)$$

where the subscript E on ξ stands for “eigenstate”. Remarkably, the difference between D and ξ_E was already realised in [34].

Now, evaluating ρ_E between any two arbitrary points in the $x - y$ plane is extremely difficult, as discussed in section 6. However, this is not strictly necessary for our purposes. With the understanding that the system is divided into network domains, with every closed domain containing a unique maximum of u , we can estimate the Agmon distance between the minima of W_E (equivalently, the maxima of u), considering only nearest neighbour domains. In other words, if we have two neighbouring domains (which share some common segment of domain walls), we aim to find the least-cost path, according to the Agmon measure, that connects the two unique maxima of u which reside in these domains. Evaluating ρ_E along this path would then be straight-forward.

Again, formally, finding the true least-cost path is a difficult task. We have found an approximate solution to this problem that seems much simpler to implement compared to all currently known alternatives, while not sacrificing much in terms of accuracy at all (see section 6 to gain perspective). As explained in appendix B of [52], the valley lines are the

paths of steepest descent, starting from each saddle point and ending at minima of u (valley lines may also terminate by exiting the system). Consider now curves that start from the saddle points and follow paths of steepest *ascent*, ending at maxima of u . Each saddle point thus links two maxima of u , and the curve formed in this way is the lowest-lying path on the inverse landscape W_E that connects the two minima of W_E in question. Figure 7 first shows an example of the valley network as originally defined [44], and then with open valley lines removed (as they do not matter for eigenstate confinement and decay) and the minimal paths connecting maxima of u through the saddle points overlaid.

We will use these paths to compute ρ_E between any two neighbouring maxima of u . First of all, we highlight that the Agmon distance is an energy-dependent quantity. Thus, along each path, the integral must be done separately at each energy of interest, E . Now, generally speaking, any two neighbouring domains have several common saddles on the shared section of their domain walls (see Fig. 7 for an example). At each energy, we must choose the minimal path which has the smallest Agmon integral out of the finite, discrete number of available options (which is computationally trivial). The path integral along that curve then becomes the Agmon distance ρ_E between the domain maxima in question at the energy considered. This must be done for all neighbouring domains and at all energies in any given landscape u .

As pointed out, ρ_E between neighbouring domains is an intrinsically energy-dependent quantity. Once the energy is so high that the saddle point of the minimal path on the effective potential W_E is below E , the cost of crossing from one domain to the other vanishes: ρ_E becomes zero as a break develops in the domain wall separating the two maxima of u (valley lines only effectively constrain eigenstates if $u < 1/E$, evaluated on the valley lines [44]). For our computation of ξ_E , we need the average of all non-zero ρ_E across the 2D system as a function of energy, but we also need to compute the domain area to extract the diameter, D . This requires integrating over the individual domain areas (at $E = 0$), averaging over all domains, assuming the area is that of a circle, and computing the diameter. However, as energy goes up and domain walls break down, domains effectively *merge*, so that the area increases with energy as well. This domain merging is fully taken into account in our calculations.

To summarise, the main steps of the calculation are as follows. Take a precomputed valley network, remove any open valley lines and calculate all the “minimal paths” connecting saddles to maxima of u . Next, identify the valley lines (and potentially segments of the system boundary) that form the domain walls for each domain and perform local, on-domain integrals (e.g. to find the domain area, in which case the integrand is one). From here, identify all saddles linking any two neighbouring domains, calculate the path integral of the Agmon distance over all linking paths between them, and finally obtain ρ_E by choosing the smallest of the integrals at every energy. Then for each noise configuration, the mean of ρ_E is computed over all neighbouring domain pairs, and the mean domain area yields the diameter D . Both of these quantities are energy dependent: zero-cost links are excluded from the average of ρ_E and domain areas are merged as the walls between them break down. Finally, many noise configurations need to be averaged over to get a reasonable estimate of the localisation length.

We remark that this calculation can be performed for any given localisation landscape as long as it has extrema. This includes, in particular, cases when the potential V is regular and Anderson localisation is impossible. The resulting “localisation length” is then of course meaningless. It is up to the researcher performing the calculation to identify cases when one is dealing with localisation before attaching any significance to the result. This can be done by

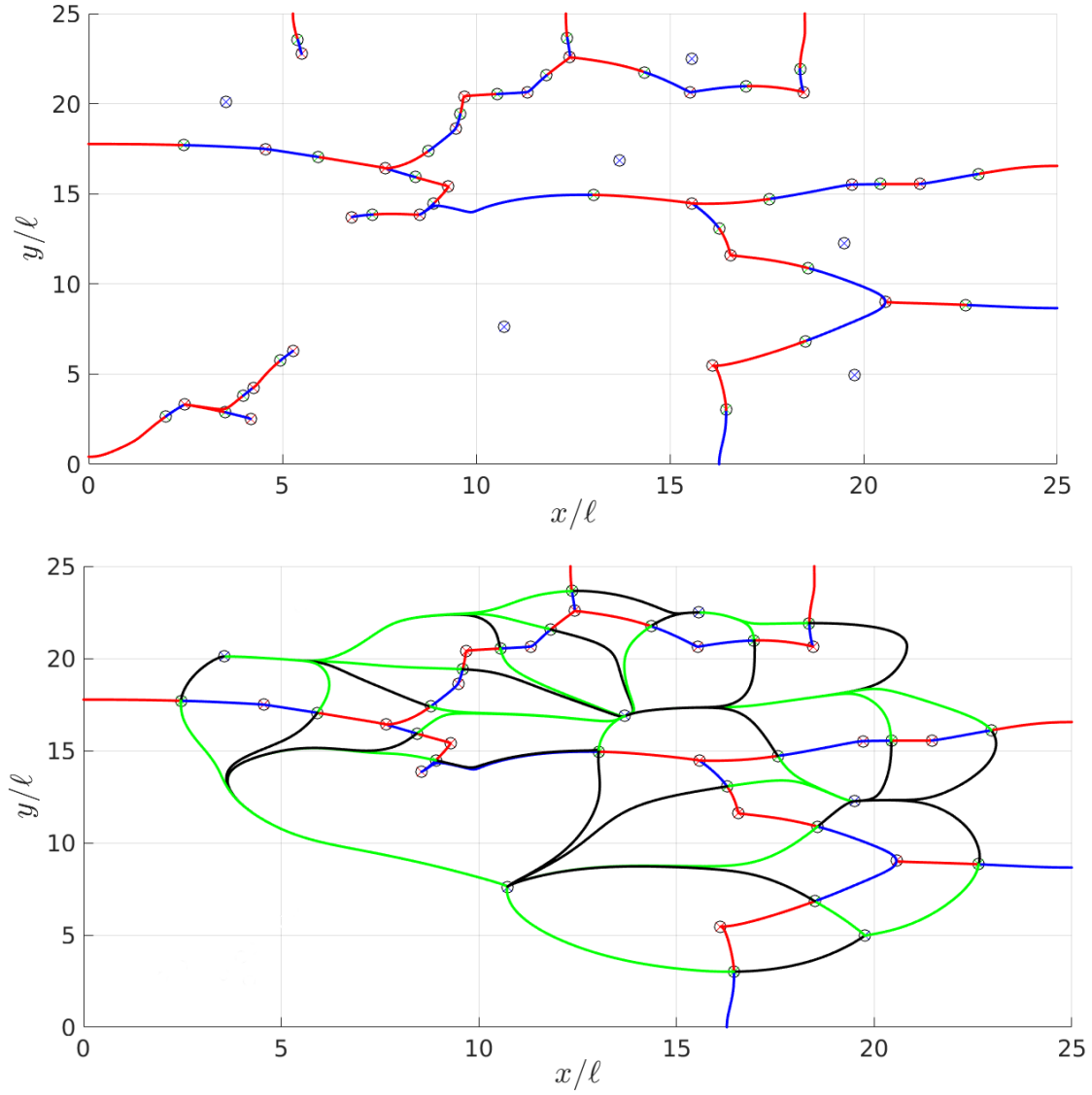


Figure 7: The original valley network (top) for some given noise realisation with $L = W = 25\ell$, $f = 0.06$, $V_0 = 5E_0$, $\sigma = \ell/2$, and the same network after all “open” valley lines have been removed (bottom). Both panels plot the valley lines in red and blue. The extrema of u are also shown as symbols (maxima in blue, minima in red, saddles in green). The bottom panel displays in addition all candidate approximate paths of least cost with respect to the Agmon metric as green and black lines, connecting neighbouring maxima of u through the linking saddle points.

examining the fundamental on-domain eigen-energies, and ensuring that they are randomised, as explained in detail in [44, 52, 60].

5.2 Test of decay constants

We have just outlined a proposed method for computing the localisation length. While there can be no question that the areas of the domains and the derived mean distance between the valley lines really give us the desired physical quantities (as long as they are calculated correctly, which has been tested), the decay constant from one domain to another, ρ_E , is a different matter entirely. As will be discussed in section 6, the level of approximation involved is very high, and there is no *a priori* assurance that our method yields numbers which faithfully capture the decay of the eigenstates. Therefore, a direct test is in order. This can be done as follows: for the same noise realisation, we perform the full LLT calculation, as well as find the low energy eigenstates by exact diagonalisation. Now, we know that within each domain, the wavefunction remains roughly constant (same order of magnitude). Therefore, we integrate $|\psi|$ over the domains, and divide by the domain areas to get the average of the wavefunction amplitude on each domain.

Then, by visual inspection of the eigenstates, we find examples of eigenstates and domain pairs where it is clear that the wavefunction tunnels from one domain to the other, as opposed to an independent occupation of the two domains. We also avoid higher local modes than the fundamental (excited local states involve nodes of the wavefunction within a domain). Having identified suitable candidates, we take the ratio of the mean amplitudes on the two domains and compute the logarithm. The resulting number is equivalent to ρ_E from LLT, the exponential cost of going specifically between these two domains (in this noise realisation), at an energy equal to the eigenvalue corresponding to the eigenstate examined.

We have performed this test, and the results are shown in Fig. 8. A clear correlation is seen, whether the predictions of LLT are compared to the eigenstates of H with potential V or W_E . The performance of the LLT method is equally good for arbitrary strengths of localisation (compare sparse and dense scatterer results), simply because the only numbers included in the test are those for which the eigenstates and domains chosen are sensible (sufficiently low energy, correct local modes, decay as opposed to independent occupation, etc.). Of course there is scatter about the identity function, but since much averaging is performed during the calculation of ξ_E , this scatter will disappear in the mean. This gives us confidence in the validity of our novel computational method.

5.3 Effect of parameters

Let us examine the localisation length obtained via the prescription given in this section. Figure 9 shows ξ_E computed from LLT for different densities of the scatterers (the same densities are examined in both panels), comparing low and high scatterers between the panels. The higher f , the smaller ξ_E , as expected. The system length in the bottom panel is twice that in top, which has the effect of increasing the localisation length due to finite size effects, as shown in Fig. 10. Finite size effects are studied methodically in [52, 61], where we find that these are visible when at least one dimension of the system is smaller than the mean distance between the valley lines. Furthermore, localisation weakens with increasing system size, but this trend is not strong and can easily be obscured by fluctuations arising from either working in a regime where finite size effects are very small, or where localisation is weak and much

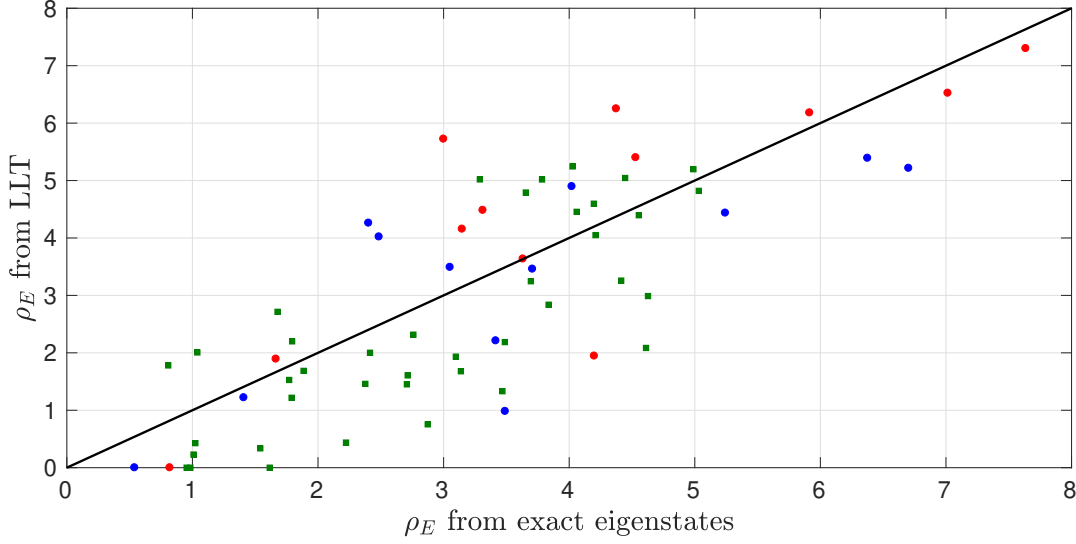


Figure 8: Exponential decay cost linking two neighbouring domains, plotting the values measured from exact eigenstates and LLT against each other. There is a very clear correlation between them: the data points fall nicely around the identity map, shown as a black solid line. All data points presented were obtained for a system with $L = W = 25\ell$, $V_0 = 21.33E_0$, $\sigma = 0.48\ell$. Blue and red circles have $f = 0.02$, with blue coming from diagonalising H with W_E and red with V , while green squares used the real potential V and $f = 0.1$.

more averaging needs to be performed to obtain accurate results. This is precisely what we see in Fig. 10: there is no clear pattern to ξ_E as L is increased at constant scatterer density, but there is always an initial increase for L changing from 25ℓ to 50ℓ . This initial increase persists at higher V_0 and higher fill factors. Despite this, it is absolutely obvious that at low V_0 the localisation length is much larger than at high V_0 (see Fig. 9). Increasing the width of the scatterers also decreases the localisation length, but we do not simulate this directly in this paper.

Each of the curves in Figs. 9 and 10 is only shown over the range of low energies where it can be trusted, i.e. where the curve is fairly smooth and monotonically increasing. We have verified that the structure seen at higher energies (in particular, the local maximum, the discontinuous jumps, etc. – see the inset of the bottom panel of Fig. 9) is all simply due to the fact the system has a finite size, combined with insufficient averaging (we use 20 noise realisations) because the network thins out so much by that point (ineffective valley lines are removed as the energy goes up). To explain, as energy increases, domains merge and their area grows in discontinuous jumps every time a domain wall breaks down. Once the average merged domain area becomes limited by system size (i.e. if the system was larger, more domains would have joined each cluster, but because there aren't any more domains, the cluster area stops growing), the calculation cannot be trusted anymore. At this point, the calculated $\xi_E(E)$ deviates from the expected monotonically increasing trend.

Furthermore, as energy increases, more and more of the domains merge and the Agmon distances linking neighbouring domains vanish. Thus the number of measurements being averaged necessarily decreases, which deteriorates the quality of the final curve. Note also

that once E exceeds all saddle points, ξ_E diverges to infinity and ceases to exist, at which point our curves must terminate. This is a predicted mobility edge, and it is studied in [52,61], where we find evidence suggesting that this prediction is unphysical. Thus, even if one could handle infinite systems numerically and remove the noise in ξ_E , we conclude in Refs. [52,61] that LLT cannot be trusted at high energies, and with it, the extracted localisation length.

As already pointed out (and demonstrated in Fig. 9), $\xi_E(E)$ depends strongly on both f and V_0 , so that one might wonder as to the precise functional form of this dependence. This is a highly non-trivial question. There is no guarantee in general that an analytical expression can be written down at all, let alone a simple one. Perhaps an expansion in an asymptotic limit could yield a simple, analytical formula for the localisation length as a function of the parameters of the noise, but obtaining accurate numerical data in these regimes is envisioned to be rather difficult. For the purpose of the present article, we mostly leave this investigation for future work, only conducting a single, simple test of the analytical formula in 2D

$$\xi \sim \ell_e \exp\left(\frac{\pi}{2} k_e \ell_e\right), \quad (9)$$

where ℓ_e is the mean free path and k_e the wavenumber associated with the energy at which the localisation length is evaluated. We recall that this formula is not expected to be entirely correct as it is derived by first assuming weak localisation and then forcing the diffusion coefficient to zero [3,4] (in addition, we do not have white noise or an infinite system).

One may relate the mean free path to the fill factor rather trivially by simple geometrical arguments, yielding $\ell_e \propto 1/\sqrt{f}$, and then fit the numerically-obtained ξ_E as a function of fill factor to

$$\xi \sim \frac{a}{\sqrt{f}} \exp\left(\frac{b}{\sqrt{f}}\right) \quad (10)$$

with energy held fixed. By examining the dependence of the fitted parameters a and b on $E \propto k_e^2$, we can judge whether the formula (9) is supported by the numerical data. We have carried out this test for a large system ($L = 75\ell$, $W = 25\ell$, well beyond the regime of visible finite-size effects [52,61]) with high scatterers ($V_0 = 21.33E_0$), varying fill factor over a wide range ($f \in [0.02, 0.2]$). An uncertainty for ξ_E may be evaluated by computing the standard error in the domain area A and the decay coefficient ρ_E , and then propagating them to find the standard error in ξ_E [see equation(8)]. Upon performing standard nonlinear fitting², we found that the coefficients a and b indeed varied smoothly with E , which was encouraging. Moreover, the b coefficient was fairly consistent with a $b \propto \sqrt{E}$ dependence, as expected from equation (9). On the other hand, a was not independent of E , as (9) predicts, but appeared to vary linearly with $1/E$. This is not only contradictory to the formula (9), but also dimensionally inconsistent, which suggests that this functional form is incorrect in our case. This is not alarming, however, because one cannot expect this formula to be applicable due to the way and the conditions under which it was derived. Thus, the true functional dependence of ξ_E on f and V_0 in our system remains an open question.

²In order to ensure the quality of each individual fit was of sufficiently high quality, we had to remove (a variable number of) the lowest fill-factor data points.

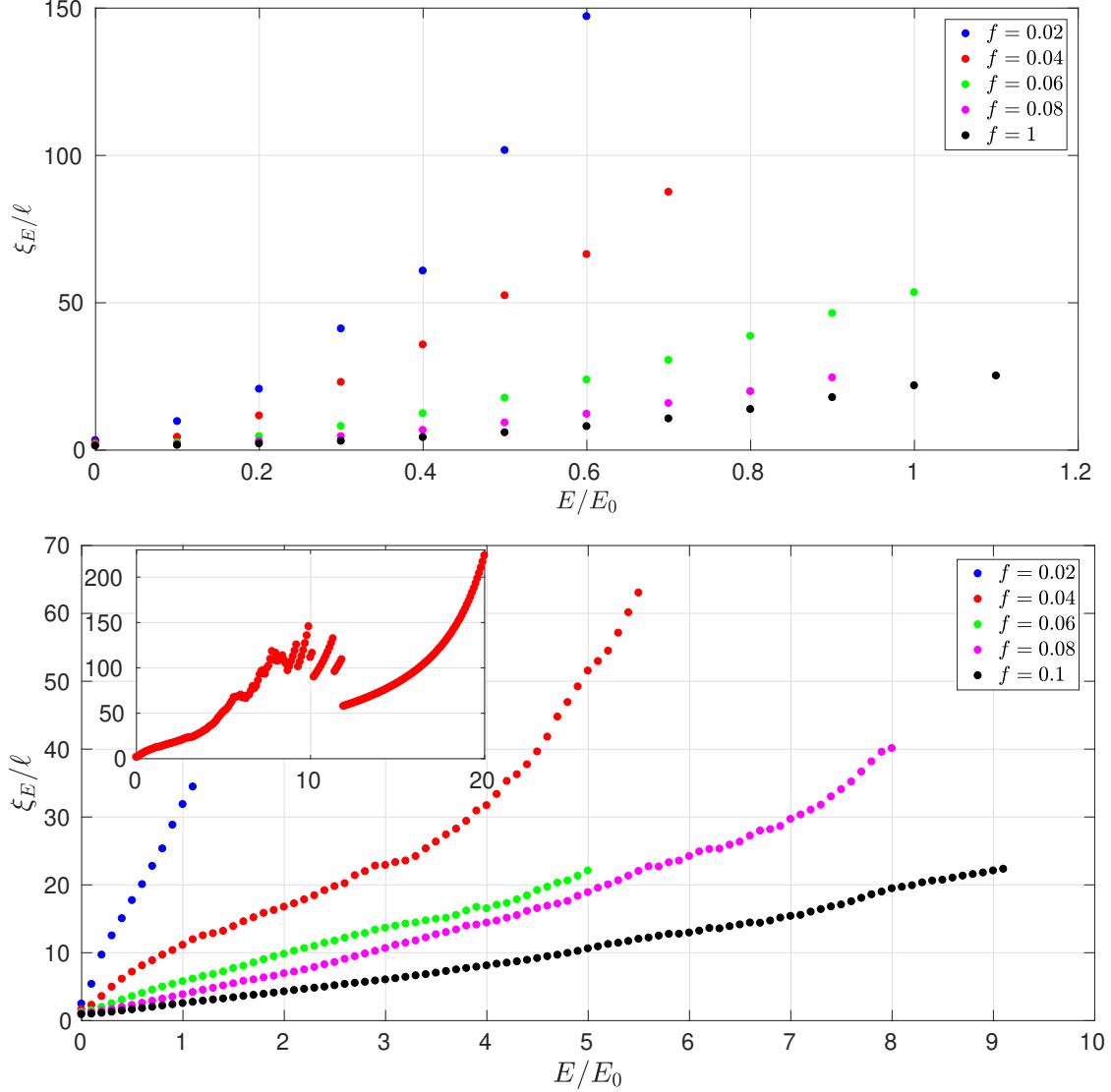


Figure 9: The eigenstate localisation length ξ_E computed for different scatterer densities (the same colour is used for the same density in both panels; see legend) and different scatterer heights: $V_0 = 5E_0$ in the top and $V_0 = 20E_0$ in the bottom panel. Other parameters are $W = 25\ell$, $\sigma = \ell/2$ common to both panels, while $L = 25\ell$ in the top and $L = 50\ell$ in the bottom panel. The inset in the bottom panel shows the $f = 0.04$ curve over a larger energy range to demonstrate the numerical noise obtained from the calculation, and the axes labels are the same as for the main figure. The localisation length increases with energy: the behaviour at high E is artificial (see inset and the text for details) and therefore is not shown for the majority of the data. In addition, ξ_E strongly decreases with increasing scatterer density and height.

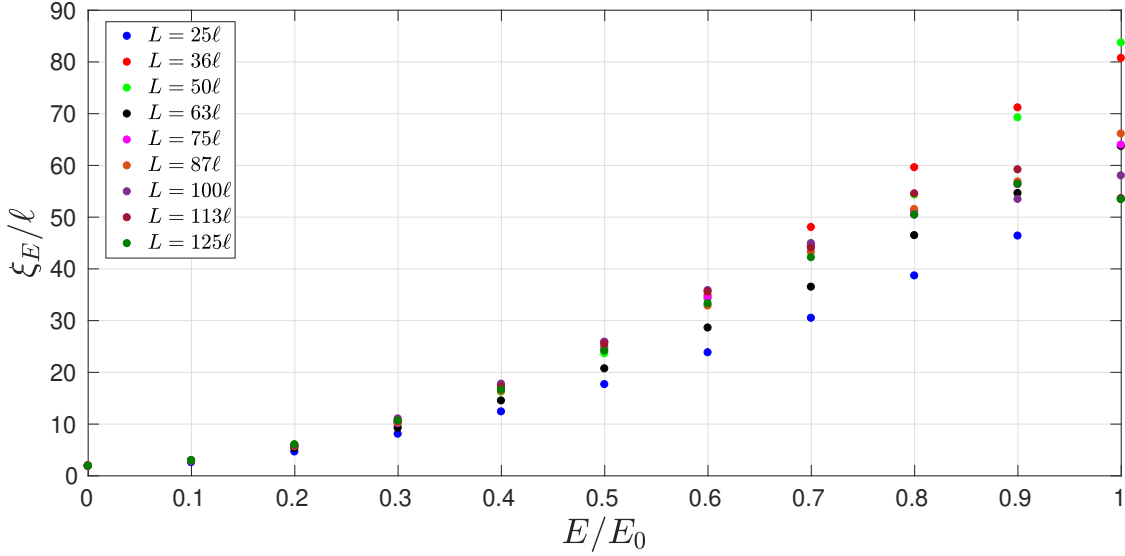


Figure 10: The eigenstate localisation length ξ_E computed for different system lengths (see legend). Other parameters are $W = 25\ell$, $\sigma = \ell/2$, $V_0 = 5E_0$, $f = 0.06$. Initially the localisation length certainly increases as L is increased (this has been confirmed in many other cases), but then there is no consistent pattern: the differences that are seen at higher L are simply fluctuations (see discussion in the main text).

6 Multidimensional tunnelling

The Agmon distance of LLT, including minimisation over all paths connecting the two points in space, gives a prescription to predict the decay of eigenstates through the barriers of W_E as they tunnel out of each domain – a local potential well – and spread across the system. In the previous section we have heuristically outlined and tested a method to quantitatively estimate ρ_E between neighbouring domain minima of W_E , avoiding the path minimisation stage, but using the usual expression for the integrand along the path.

Multidimensional tunnelling is in fact an old and thoroughly-investigated problem. Of course, brute force quantum mechanical calculations are possible, but physicists have been striving to obtain *insight* into the process by generalising the WKB approximation to dimensions higher than one to describe it. In 1D, WKB is a straight-forward and methodical approach (see, e.g., [62]) – a controlled approximation that is fully understood. The generalisation to several dimensions is a different matter entirely: there is a large body of literature developing and discussing different methods, their limitations, suggesting improvements, and utilising these techniques to solve practical problems. In this section, we will provide an overview of this topic, to place our method of section 5 in perspective.

Let us see where the Agmon distance equation (6) comes from. The starting point of the derivation is usually the Feynman propagator, none other than the Green's function of the system. One has to go through a series of approximations, listed below, in order to arrive at this semi-classical formalism:

1. The propagator is expanded in powers of \hbar , and only the zeroth order term is retained³

³An equivalent approach is to write the wavefunction in polar form and expand the phase similarly.

[63, 64].

2. Next, one usually assumes that Hamilton’s principle function is pure imaginary [63, 65, 66].
3. In principle, if we want to use the Feynman propagator to describe tunnelling from one region of space where the wavefunction is initially contained to another, we must consider all source points, all target points, and all possible paths to arrive from each source to each target point. In the simplest approximation, one uses the fact that the contribution of the classical path is the largest, and as we move away from it in configuration space, the contribution of the other paths is exponentially suppressed. Therefore, one usually only examines the classical path, or at most a “tube” of paths around the classical one. Moreover, it is common to only consider one source point (at which the wavefunction is maximal) and one target point (say the minimum in the potential on the other side of the barrier). The classical trajectory method was developed and used in many papers, e.g. [64, 67–69], and relies on minimising the action via the Euler-Lagrange equations.

Assumption 1 is already a strong limitation, and to the best of our knowledge, first order solutions were only ever obtained in the classically allowed region [63]. However, taking $\hbar \rightarrow 0$ is the essence of the semi-classical nature of the method, and not much can be practically done to overcome this approximation.

Assumption 2 is certainly not generally justified [63, 65, 66]. These three references have superbly dealt with the case of a general complex action, and demonstrated that a geometrical ray construction, following two surfaces (equi-phase and equi-amplitude) along two orthogonal paths, is necessary to solve the problem in earnest. They have proven that the imaginary action approximation breaks down if one considers a general incoming wavefunction, incident on a barrier such that its k -vector is arbitrarily predetermined. It has also been argued that this approximation can even fail for tunnelling out of a potential well [66]. The geometrical construction proposed in these papers is extremely involved, and completely impractical for our purposes.

While in principle, accuracy could be improved by including more than one source and target point, as well as considering multiple paths as in [64], all three simplifications of the third assumption are essential for our case: we cannot afford (computationally) to calculate many paths or to describe each domain by anything more than the point at which W_E attains its minimum. This is simply because the calculation needs to be done so *many* times that it is simply impractical.

The usual final form of the semi-classical approximation in the forbidden region involves solving the classical equations of motion with negative the potential and the energy, or equivalently, in imaginary time. The differential equations are based on Newton’s laws, imposing energy conservation as a constraint, and seek out the path of minimal action. In the context of tunnelling out of a potential well, the trajectory is usually required to pass through the turning surface (where the kinetic energy vanishes) normally, so that it can connect smoothly to a classical trajectory in the allowed region. On the turning surface, the velocity is aligned along the gradient of the potential [64, 69]. An alternative constraint was used in [67]: the authors required their escape paths to pass through the saddles of the potential and be aligned along the correct axis of the saddle at those points (which is closer in spirit to our approach, but is less rigorous). Essentially, if the direction of the incoming wave is predetermined and it impinges on the turning surface at any angle other than normally, the action must be taken

as complex and the classical equations are insufficient. This is the chief difference between tunnelling out of a local well and the transmission of an incoming wave through a barrier.

We highlight that in the final form of the semi-classical approximation, the minimal path is energy-dependent: one must solve the set of ordinary differential equations defining the minimal path for each energy separately. If we wish to find the classical path that connects two specific points, knowledge of the energy gives us the magnitude of the velocity vector, but its direction is unknown. Trial and error is called for to discover the latter: one needs to try different initial directions of motion until a path that arrives at the desired end point is found. This makes the traditional (and formally correct) solution of the semi-classical problem impractical for our purposes.

Our method of section 5 overcomes these problems: no differential equations need to be solved at all (one only needs to know the localisation landscape u), one path is computed for all energies, and there is no need to guess the initial condition. As we have seen in Fig. 8, it performs well, which justifies its use despite the many approximations in deriving the semi-classical formulation, as well as our heuristic way of computing the escape paths. In either case, no other level of approximation is practical for our purposes, as we need to compute the Agmon distance between every two neighbouring domains at all energies for many noise realisations (twenty are used in practice), at each set of parameters investigated.

A few final notes are in order, without which any review of multidimensional tunnelling would be incomplete. References [70, 71] have developed the path decomposition expansion method, which allows one to divide space into separate regions, minimise the action in each region using whatever method happens to be optimal in that region (chosen based on physical considerations), and then collate the solutions using global consistency equations. While not used in our work, it is clear that our problem would fit nicely into such a formalism: our system is naturally divided into domains (which are local basins in W_E). It should be possible to use the path decomposition expansion formalism to predict tunnelling across large distances, spanning several domains, by combining local information through global collocation equations.

Reference [64] deserves special attention, as an exceptional effort was made to consider many classical paths from many source points, deriving the tunnelling current and transmission coefficient through the potential barrier.

For a more comprehensive review of the topic, the reader is referred to [72], as well as the original literature cited above.

7 Conclusions and future work

In this paper we used LLT to calculate the eigenstate localisation length, quantifying the decay length scale of the eigenstates, as a function of energy. This required us to develop a practical approximation to multidimensional tunnelling and a formidable extension of LLT techniques and machinery. It also involved considerable conceptual progress, linking together domain size and the decay exponent (the “cost”) of tunnelling through the peak ranges of W_E separating domains through the saddle points. We accounted for the effect of increasing energy by merging domains as the domain walls separating them broke down. Crucially, we explicitly tested the decay coefficients computed from LLT against exact eigenstates, validating our computational method and the many approximations involved. We also reviewed

multidimensional tunnelling to set our method in context.

In addition, we highlighted the difficulty in extracting the localisation length out of exact diagonalisation calculations. We further demonstrated that the effective potential W_E can replace the real potential V in the Hamiltonian in terms of reproducing the low-energy eigenspectrum as well as for time-evolution of expanding or transmitting wavepackets.

Some ideas for future work that naturally came up during this investigation are:

1. First of all, it would be excellent to generalise LLT to 3D, where the logic and conceptual picture are largely unchanged, but the practical framework and the technology are not yet in place (everything beyond obtaining u and performing simple mathematical operations on it). This would open the door to a large number of possible studies in 3D.
2. One should also investigate the functional dependence of ξ_E on the fill factor and V_0 . At the moment, this can only be done by running large numbers of simulations at different parameters and examining the dependence explicitly, hoping to discover the functional form by inspection.
3. What effect does the shape of the scatterers have? We have limited ourselves to 2D Gaussian peaks (of more or less constant width) for this paper. What would happen if we changed the width, or even made the scatterers, say, square?

Acknowledgements

S.S.S. warmly thanks the following researchers for extremely helpful discussions on the topics indicated in parentheses after each name: Daniel V. Shamailov (the entire project), Antonio Mateo-Munõz (spectral methods in exact diagonalisation), Xiaoquan Yu (importance of the density of states for Anderson localisation), Marcel Filoche and Svitlana Mayboroda (the Agmon distance). Jan Major is further gratefully acknowledged for reading the manuscript and providing useful comments.

References

- [1] S. C.M. and E. Economou, *Electronic localization in disordered systems*, Waves in Random Media **9**(2), 255 (1999), doi:10.1088/0959-7174/9/2/310, <https://doi.org/10.1088/0959-7174/9/2/310>.
- [2] P. W. Anderson, *Absence of diffusion in certain random lattices*, Phys. Rev. **109**, 1492 (1958), doi:10.1103/PhysRev.109.1492.
- [3] P. Sheng, *Introduction to Wave Scattering, Localization and Mesoscopic Phenomena*, Springer Series in MATERIALS SCIENCE, Volume 88. Springer-Verlag Berlin Heidelberg, doi:10.1007/3-540-29156-3 (2006).
- [4] P. Wölfle and D. Vollhardt, *Self-consistent theory of anderson localization: General formalism and applications*, International Journal of Modern Physics B

- 24**(12n13), 1526 (2010), doi:10.1142/S0217979210064502, <https://doi.org/10.1142/S0217979210064502>.
- [5] M. Piraud, A. Aspect and L. Sanchez-Palencia, *Anderson localization of matter waves in tailored disordered potentials*, Phys. Rev. A **85**, 063611 (2012), doi:10.1103/PhysRevA.85.063611.
- [6] R. C. Kuhn, C. Miniatura, D. Delande, O. Sigwarth and C. A. Müller, *Localization of matter waves in two-dimensional disordered optical potentials*, Phys. Rev. Lett. **95**, 250403 (2005), doi:10.1103/PhysRevLett.95.250403.
- [7] W. Morong and B. DeMarco, *Simulation of anderson localization in two-dimensional ultracold gases for pointlike disorder*, Phys. Rev. A **92**, 023625 (2015), doi:10.1103/PhysRevA.92.023625.
- [8] I. Manai, J.-F. m. c. Clément, R. Chicireanu, C. Hainaut, J. C. Garreau, P. Szriftgiser and D. Delande, *Experimental observation of two-dimensional anderson localization with the atomic kicked rotor*, Phys. Rev. Lett. **115**, 240603 (2015), doi:10.1103/PhysRevLett.115.240603.
- [9] V. Gasparian and A. Suzuki, *Localization length in two-dimensional disordered systems: effects of evanescent modes*, Journal of Physics: Condensed Matter **21**(40), 405302 (2009), doi:10.1088/0953-8984/21/40/405302.
- [10] Y. Ono, *Self-consistent theory of anderson localization: Magnetic field effects*, Progress of Theoretical Physics Supplement **84**, 138 (1985), doi:10.1143/PTPS.84.138, <https://academic.oup.com/ptps/article-pdf/doi/10.1143/PTPS.84.138/5164032/84-138.pdf>.
- [11] K. L. Lee, B. Grémaud, C. Miniatura and D. Delande, *Analytical and numerical study of uncorrelated disorder on a honeycomb lattice*, Phys. Rev. B **87**, 144202 (2013), doi:10.1103/PhysRevB.87.144202.
- [12] D. J. Thouless, *A relation between the density of states and range of localization for one dimensional random systems*, Journal of Physics C: Solid State Physics **5**(1), 77 (1972), doi:10.1088/0022-3719/5/1/010.
- [13] H. De Raedt, A. Lagendijk and P. de Vries, *Transverse localization of light*, Phys. Rev. Lett. **62**, 47 (1989), doi:10.1103/PhysRevLett.62.47.
- [14] D. H. White, T. A. Haase, D. J. Brown, M. D. Hoogerland, M. S. Najafabadi, J. L. Helm, C. Gies, D. Schumayer and D. A. Hutchinson, *Observation of two-dimensional anderson localisation of ultracold atoms*, arXiv:1911.04858 (2019).
- [15] S. Donsa, H. Hofstätter, O. Koch, J. Burgdörfer and I. Březinová, *Long-time expansion of a bose-einstein condensate: Observability of anderson localization*, Phys. Rev. A **96**, 043630 (2017), doi:10.1103/PhysRevA.96.043630.
- [16] A. Peres, M. Revzen and A. Ron, *Calculation of localization length in disordered chains*, Phys. Rev. B **24**, 7463 (1981), doi:10.1103/PhysRevB.24.7463.

- [17] H. Eleuch and M. Hilke, *Localization and delocalization for strong disorder in one-dimensional continuous potentials*, New Journal of Physics **17**(8), 083061 (2015), doi:10.1088/1367-2630/17/8/083061.
- [18] A. Gharaati, F. Bahadori and H. Boroumandi, *Calculation of anderson localization length by using generalized quantum kicked rotator analytically*, ACTA PHYSICA POLONICA A **121**(1), 30 (2012).
- [19] S. Kettemann, *Dimensional crossover of localization and delocalization in a quantum hall bar*, Phys. Rev. B **69**, 035339 (2004), doi:10.1103/PhysRevB.69.035339.
- [20] R. Johnston and H. Kunz, *A method for calculating the localisation length, with an analysis of the lloyd model*, Journal of Physics C: Solid State Physics **16**(23), 4565 (1983), doi:10.1088/0022-3719/16/23/018.
- [21] J. L. Pichard and G. Sarma, *Finite size scaling approach to anderson localisation*, Journal of Physics C: Solid State Physics **14**(6), L127 (1981), doi:10.1088/0022-3719/14/6/003.
- [22] J. Heinrichs, *Localization length in dorokhov s microscopic model of multi-channel wires*, Journal of Physics: Condensed Matter **15**(29), 5025 (2003), doi:10.1088/0953-8984/15/29/314.
- [23] Z. Fan, A. Uppstu and A. Harju, *Anderson localization in two-dimensional graphene with short-range disorder: One-parameter scaling and finite-size effects*, Phys. Rev. B **89**, 245422 (2014), doi:10.1103/PhysRevB.89.245422.
- [24] A. Eilmes, R. R.A. and M. Schreiber, *The two-dimensional anderson model of localization with random hopping*, Eur. Phys. J. B **1**, 29 (1998), doi:https://doi.org/10.1007/s100510050149.
- [25] A. Eilmes and R. A. Römer, *Exponents of the localization length in the 2d anderson model with off-diagonal disorder*, physica status solidi (b) **241**(9), 2079 (2004), doi:10.1002/pssb.200404793, <https://onlinelibrary.wiley.com/doi/pdf/10.1002/pssb.200404793>.
- [26] A. MacKinnon and B. Kramer, *The scaling theory of electrons in disordered solids: Additional numerical results*, Zeitschrift für Physik B Condensed Matter **53**(1), 1 (1983), doi:10.1007/BF01578242.
- [27] Y. Su, C. Wang, Y. Avishai, Y. Meir and X. R. Wang, *Absence of localization in disordered two-dimensional electron gas at weak magnetic field and strong spin-orbit coupling*, Scientific Reports **6**, 33304 (2016), doi:10.1038/srep33304.
- [28] Liu, Wen-Sheng, Liu, S. Y. and Lei, X. L., *Metal-insulator transition in two-dimensional systems with long-range correlated disorder*, Eur. Phys. J. B **33**(3), 293 (2003), doi:10.1140/epjb/e2003-00169-4.
- [29] P. D. Kirkman and J. B. Pendry, *The statistics of one-dimensional resistances*, Journal of Physics C: Solid State Physics **17**(24), 4327 (1984), doi:10.1088/0022-3719/17/24/014.
- [30] S. Derevyanko, *Anderson localization of a one-dimensional quantum walker*, Scientific Reports **8**, 1795 (2018), doi:10.1038/s41598-017-18498-1.

- [31] P. A. Lee and D. S. Fisher, *Anderson localization in two dimensions*, Phys. Rev. Lett. **47**, 882 (1981), doi:10.1103/PhysRevLett.47.882.
- [32] E. Abrahams, P. W. Anderson, D. C. Licciardello and T. V. Ramakrishnan, *Scaling theory of localization: Absence of quantum diffusion in two dimensions*, Phys. Rev. Lett. **42**, 673 (1979), doi:10.1103/PhysRevLett.42.673.
- [33] D. C. Herbert and R. Jones, *Localized states in disordered systems*, Journal of Physics C: Solid State Physics **4**(10), 1145 (1971), doi:10.1088/0022-3719/4/10/023.
- [34] E. Economou and C. Papatrantafillou, *Localization lengths in one-dimensional disordered systems*, Solid State Communications **11**(1), 197 (1972), doi:https://doi.org/10.1016/0038-1098(72)91161-1.
- [35] H. Aoki, *Real-space renormalisation-group theory for anderson localisation: decimation method for electron systems*, Journal of Physics C: Solid State Physics **13**(18), 3369 (1980), doi:10.1088/0022-3719/13/18/006.
- [36] H. He, *Localization length of wave functions in one-dimensional disordered systems with second nearest neighbour couplings*, Solid State Communications **67**(3), 243 (1988), doi:https://doi.org/10.1016/0038-1098(88)90609-6.
- [37] J. Mertsching, *Density of states and localization length in weakly disordered peierls chains*, Synthetic Metals **57**(2), 4602 (1993), doi:https://doi.org/10.1016/0379-6779(93)90789-Y.
- [38] S.-J. Xiong and Y. Xiong, *Anderson localization of electron states in graphene in different types of disorder*, Phys. Rev. B **76**, 214204 (2007), doi:10.1103/PhysRevB.76.214204.
- [39] F. Domínguez-Adame and V. A. Malyshev, *A simple approach to anderson localization in one-dimensional disordered lattices*, American Journal of Physics **72**(2), 226 (2004), doi:10.1119/1.1593660.
- [40] D. Weaire and V. Srivastava, *Numerical results for anderson localisation in the presence of off-diagonal disorder*, Solid State Communications **23**(11), 863 (1977), doi:https://doi.org/10.1016/0038-1098(77)90970-X.
- [41] E. Economou and P. Antoniou, *Localization and off-diagonal disorder*, Solid State Communications **21**(3), 285 (1977), doi:https://doi.org/10.1016/0038-1098(77)90188-0.
- [42] F. A. de Moura and M. L. Lyra, *Correlation-induced metal-insulator transition in the one-dimensional anderson model*, Physica A: Statistical Mechanics and its Applications **266**(1), 465 (1999), doi:https://doi.org/10.1016/S0378-4371(98)00632-3.
- [43] F. Izrailev, A. Krokhin and N. Makarov, *Anomalous localization in low-dimensional systems with correlated disorder*, Physics Reports **512**(3), 125 (2012), doi:https://doi.org/10.1016/j.physrep.2011.11.002.
- [44] M. Filoche and S. Mayboroda, *Universal mechanism for anderson and weak localization*, Proceedings of the National Academy of Sciences **109**(37), 14761 (2012), doi:10.1073/pnas.1120432109, <https://www.pnas.org/content/109/37/14761.full.pdf>.

- [45] M. L. Lyra, S. Mayboroda and M. Filoche, *Dual landscapes in anderson localization on discrete lattices*, EPL (Europhysics Letters) **109**(4), 47001 (2015), doi:10.1209/0295-5075/109/47001.
- [46] G. Lefebvre, A. Gondel, M. Dubois, M. Atlan, F. Feppon, A. Labbé, C. Gillot, A. Garelli, M. Ernoult, S. Mayboroda, M. Filoche and P. Sebbah, *One single static measurement predicts wave localization in complex structures*, Phys. Rev. Lett. **117**, 074301 (2016), doi:10.1103/PhysRevLett.117.074301.
- [47] D. N. Arnold, G. David, D. Jerison, S. Mayboroda and M. Filoche, *Effective confining potential of quantum states in disordered media*, Phys. Rev. Lett. **116**, 056602 (2016), doi:10.1103/PhysRevLett.116.056602.
- [48] M. Filoche, M. Piccardo, Y.-R. Wu, C.-K. Li, C. Weisbuch and S. Mayboroda, *Localization landscape theory of disorder in semiconductors. i. theory and modeling*, Phys. Rev. B **95**, 144204 (2017), doi:10.1103/PhysRevB.95.144204.
- [49] M. Piccardo, C.-K. Li, Y.-R. Wu, J. S. Speck, B. Bonef, R. M. Farrell, M. Filoche, L. Martinelli, J. Peretti and C. Weisbuch, *Localization landscape theory of disorder in semiconductors. ii. urbach tails of disordered quantum well layers*, Phys. Rev. B **95**, 144205 (2017), doi:10.1103/PhysRevB.95.144205.
- [50] C.-K. Li, M. Piccardo, L.-S. Lu, S. Mayboroda, L. Martinelli, J. Peretti, J. S. Speck, C. Weisbuch, M. Filoche and Y.-R. Wu, *Localization landscape theory of disorder in semiconductors. iii. application to carrier transport and recombination in light emitting diodes*, Phys. Rev. B **95**, 144206 (2017), doi:10.1103/PhysRevB.95.144206.
- [51] W. Hahn, J.-M. Lentali, P. Polovodov, N. Young, S. Nakamura, J. S. Speck, C. Weisbuch, M. Filoche, Y.-R. Wu, M. Piccardo, F. Maroun, L. Martinelli *et al.*, *Evidence of nanoscale anderson localization induced by intrinsic compositional disorder in ingan/gan quantum wells by scanning tunneling luminescence spectroscopy*, Phys. Rev. B **98**, 045305 (2018), doi:10.1103/PhysRevB.98.045305.
- [52] S. S. Shamilov, D. J. Brown, T. A. Haase and M. D. Hoogerland, *Anderson localisation in two dimensions: insights from localisation landscape theory, exact diagonalisation, and time-dependent simulations*, arXiv:2003.00149 (2020).
- [53] G. Roati, C. D’Errico, L. Fallani, M. Fattori, C. Fort, M. Zaccanti, G. Modugno, M. Modugno and M. Inguscio, *Anderson localization of a non-interacting bose-einstein condensate*, Nature **453**, 895 (2008), doi:10.1038/nature07071.
- [54] G. Semeghini, M. Landini, P. Castilho, S. Roy, G. Spagnolli, A. Trenkwalder, M. Fattori, M. Inguscio and G. Modugno, *Measurement of the mobility edge for 3d anderson localization*, Nature Physics **11**, 554 (2015), doi:10.1038/nphys3339.
- [55] D. Clément, A. F. Varón, M. Hugbart, J. A. Retter, P. Bouyer, L. Sanchez-Palencia, D. M. Gangardt, G. V. Shlyapnikov and A. Aspect, *Suppression of transport of an interacting elongated bose-einstein condensate in a random potential*, Phys. Rev. Lett. **95**, 170409 (2005), doi:10.1103/PhysRevLett.95.170409.

- [56] M. Robert-de Saint-Vincent, J.-P. Brantut, B. Allard, T. Plisson, L. Pezzé, L. Sanchez-Palencia, A. Aspect, T. Bourdel and P. Bouyer, *Anisotropic 2d diffusive expansion of ultracold atoms in a disordered potential*, Phys. Rev. Lett. **104**, 220602 (2010), doi:10.1103/PhysRevLett.104.220602.
- [57] F. Jendrzejewski, A. Bernard, K. Müller, P. Cheinet, V. Josse, M. Piraud, L. Pezzé, L. Sanchez-Palencia and P. Aspect, A. Bouyer, *Three-dimensional localization of ultracold atoms in an optical disordered potential*, Nature Physics **8**, 398 (2011), doi:10.1038/nphys2256.
- [58] G. Berthet, L. Lavoine, M. K. Parit, A. Brolis, A. Boissé and T. Bourdel, *Observation of the algebraic localization-delocalization transition in a one-dimensional disordered potential with a bias force*, Phys. Rev. Research **2**, 013386 (2020), doi:10.1103/PhysRevResearch.2.013386.
- [59] S. S. Shamailov, D. J. Brown, T. A. Haase and M. D. Hoogerland, *Transmitting translating gaussian wavepackets through disordered potentials as a method of detecting and studying anderson localisation*, to be published.
- [60] S. S. Shamailov, D. J. Brown, T. A. Haase and M. D. Hoogerland, *Understanding and identifying the role of disorder in anderson localisation*, to be published.
- [61] S. S. Shamailov, D. J. Brown, T. A. Haase and M. D. Hoogerland, *Dimensional crossover, mobility edge and expansion versus transmission in two-dimensional anderson-localised systems*, to be published.
- [62] S. K. Knudson and D. W. Noid, *The multidimensional wkb method*, Journal of Chemical Education **66**(2), 133 (1989), doi:10.1021/ed066p133, <https://doi.org/10.1021/ed066p133>.
- [63] Z. H. Huang, T. E. Feuchtwang, P. H. Cutler and E. Kazes, *Wentzel-kramers-brillouin method in multidimensional tunneling*, Phys. Rev. A **41**, 32 (1990), doi:10.1103/PhysRevA.41.32.
- [64] B. Das and J. Mahanty, *Spatial distribution of tunnel current and application to scanning-tunneling microscopy: A semiclassical treatment*, Phys. Rev. B **36**, 898 (1987), doi:10.1103/PhysRevB.36.898.
- [65] P. Bowcock and R. Gregory, *Multidimensional tunneling and complex momentum*, Phys. Rev. D **44**, 1774 (1991), doi:10.1103/PhysRevD.44.1774.
- [66] S. Takada and H. Nakamura, *Wentzel-kramers-brillouin theory of multidimensional tunneling: General theory for energy splitting*, The Journal of Chemical Physics **100**(1), 98 (1994), doi:10.1063/1.466899, <https://doi.org/10.1063/1.466899>.
- [67] T. Banks, C. M. Bender and T. T. Wu, *Coupled anharmonic oscillators. i. equal-mass case*, Phys. Rev. D **8**, 3346 (1973), doi:10.1103/PhysRevD.8.3346.
- [68] T. Banks and C. M. Bender, *Coupled anharmonic oscillators. ii. unequal-mass case*, Phys. Rev. D **8**, 3366 (1973), doi:10.1103/PhysRevD.8.3366.

- [69] S. Coleman, *Fate of the false vacuum: Semiclassical theory*, Phys. Rev. D **15**, 2929 (1977), doi:10.1103/PhysRevD.15.2929.
- [70] A. Auerbach, S. Kivelson and D. Nicole, *Path decomposition for multidimensional tunneling*, Phys. Rev. Lett. **53**, 411 (1984), doi:10.1103/PhysRevLett.53.411.
- [71] A. Auerbach and S. Kivelson, *The path decomposition expansion and multidimensional tunneling*, Nuclear Physics B **257**, 799 (1985), doi:https://doi.org/10.1016/0550-3213(85)90377-3.
- [72] K. Takatsuka, H. Ushiyama and A. Inoue-Ushiyama, *Tunneling paths in multi-dimensional semiclassical dynamics*, Physics Reports **322**(5), 347 (1999), doi:https://doi.org/10.1016/S0370-1573(99)00036-8.